# Thermodynamics and Equilibrium Solubility of Carbon Dioxide in Diglycolamine/Morpholine/Water

**Mohammed Al-Juaied[†] and Gary T. Rochelle***

Department of Chemical Engineering, The University of Texas at Austin, Austin, Texas 78712

Carbon dioxide solubility was studied in 3.5 m (23.5 wt %) morpholine (MOR), 17.7 m (65 wt %) 2-aminoethoxyethanol (diglycolamine or DGA), and 3.6 m MOR + 14.7 m DGA (11 wt % MOR + 53 wt % DGA). $CO_2$ solubility was determined by dynamic measurements with a wetted wall contactor. Carbamate and bicarbonate concentrations were determined by $^{13}C$ NMR in solutions loaded with $^{13}CO_2$. The data are represented by the electrolyte NRTL model. At a given $CO_2$ loading (mol/mol amine), the $CO_2$ vapor pressure over 3.5 m MOR is 10 to 1000 times greater than 17.7 m DGA. In 3.6 m MOR + 14.7 m DGA, the $CO_2$ vapor pressure is 5 to 7 times greater than in 17.7 m DGA at high $CO_2$ loading, but the same below 0.2 loading. MOR carbamate is less stable than DGA carbamate by a factor of 7 to 10 from (300 to 333) K. The model predicts that MOR vapor pressure is 100 times greater than DGA over 3.6 m MOR + 14.7 m DGA from (313 to 333) K. The heat of $CO_2$ absorption in the blend is equivalent to 17.7 m DGA up to 0.35 loading but is 40 % lower at 0.5 loading. The working capacity of the blend is 17 % less than 17.7 m DGA.

## Introduction

$CO_2$ is removed from natural gas by absorbing/stripping with aqueous 2-aminoethoxyethanol (diglycolamine DGA). DGA systems are normally installed with reclaimers to maintain solvent quality by reducing corrosion, foaming, and degradation of the solvent. Two plants at Saudi Aramco have shown that DGA reacts with its carbamate to produce reversibly *N,N*′-bis-(hydroxyethoxyethyl)urea, which can thermally degrade in the reclaimer to produce morpholine (MOR).[1]

Thermodynamic data and models are useful in predicting the performance of DGA with varying amounts of MOR. The electrolyte NRTL framework that has been developed to represent blends of tertiary amines with primary or secondary amines can be further modified to represent blends of DGA and MOR.

Limited $CO_2$ solubility data are available for DGA. This work obtains additional data for DGA and new data for MOR and the blend. Previous investigators have used $^{13}C$ NMR to speciate loaded amine solutions, but no data are available for DGA or MOR. This paper presents speciation results for DGA/MOR/$CO_2$/$H_2O$ with $^{13}C$ NMR.

Blended amine solvents have been studied by several researchers. Austgen[2] studied the thermodynamics of methyldiethanolamine (MDEA) blends with MEA, DEA, and DGA using the electrolyte NRTL model. Posey[3] improved the models by studying the activity coefficient of the amines at infinite dilution. Pacheco et al.[4] studied the absorption of $CO_2$ into aqueous DGA + MDEA. Glasscock[5] and Critchfield[6] have studied DEA + MDEA and MEA + MDEA. Specifically, this work will use the thermodynamic frameworks presented by Bishnoi and Rochelle,[7] Austgen et al.,[8] and Posey and Rochelle[9] to represent new data, previous VLE data,[10,11] and $N_2O$ solubility data[12] for DGA and MOR. Parameters of the electrolyte NRTL model

were adjusted to match $CO_2$ solubility data, $^{13}C$ NMR data, and $N_2O$ solubility data. The fitted model was then used to estimate solvent working capacity, heat of reaction, and vaporization losses for DGA and MOR + DGA.

## Experimental Methods

Solubility of $CO_2$ was determined using wetted wall apparatus and methodology most recently used by Bishnoi.[13] Absorption and desorption data are bracketed, and flux is interpolated to zero to determine the equilibrium partial pressure of $CO_2$ at a given $CO_2$ loading. Samples of the liquid demonstrate that the loading has not changed during the absorption and desorption events. $CO_2$ gas concentration was determined continuously by two infrared analyzers (HORIBA model PIR-2000) in series with ranges of 0 to 1 and 0 to 25 % $CO_2$. Solutions were prepared gravimetrically from commercial-grade MOR and DGA with purity greater than 99 %. The amount of total $CO_2$ (free $CO_2$ plus chemically combined) in the liquid phase was determined with a precision of 5 % using a total carbon analyzer, model 525 from Oceanography International Corporation. The gage pressure was measured using an Ashcroft pressure gauge, 0 to 140 kPa at ± 0.14 kPa. J-type thermocouples were used in the solution inlet and outlet lines to the reactor with an accuracy of ± 0.5 K. The average of the inlet and outlet temperatures is reported here.

Measurements of $^{13}C$ nuclear magnetic resonance (NMR) were performed at (300, 313, and 333) K on a Varian INOVA-500. Solutions were prepared by sparging $^{13}CO_2$ into $D_2O$ solutions of the respective amine. The NMR spectra were acquired with a relaxation delay of five times the relaxation time to ensure quantitative signals. Peak areas, derived from both $^{13}CO_2$ and natural $^{13}C$, were integrated and used to determine the relative concentration of chemical species present in solution.

## Model Description

A flexible FORTRAN code for the solution and phase equilibrium of acid gas systems was developed by Austgen.[2]
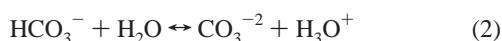
* To whom correspondence should be addressed. Tel.: (512)471-7230. Fax: (512)475-7824. E-mail: gtr@che.utexas.edu.
[†] Current address: Saudi Aramco, Dharan, Saudi Arabia.

**Table 1. Default Parameters for VLE Calculation**

| parameter | $A$ | $B$ | $\alpha$ |
|---|---|---|---|
| molecule/molecule | 0 | 0 | 0.2 |
| water/salt pair | 8.0 | 0 | 0.2 |
| salt pair/water | −4.0 | 0 | 0.2 |
| all molecules (other than water)/salt pair | 15.0 | 0 | 0.1 |
| all salt pair/molecule (other than water) | −8.0 | 0 | 0.1 |

This code was modified to model MOR, DGA, and MOR + DGA. The model uses the Smith and Missen[14] nonstoichiometric algorithm to speciate the liquid solution. Equilibrium constants were used to calculate the standard state chemical potentials using the method described by Austgen.[2] The following reactions and species are considered:

$$CO_2(aq) + 2H_2O \leftrightarrow HCO_3^- + H_3O^+ \qquad (1)$$

$$HCO_3^- + H_2O \leftrightarrow CO_3^{-2} + H_3O^+ \qquad (2)$$

$$2H_2O \leftrightarrow H_3O^+ + OH^- \qquad (3)$$

$$MORH^+ + H_2O \leftrightarrow MOR + H_3O^+ \qquad (4)$$

$$MOR + CO_2 + H_2O \leftrightarrow MORCOO^- + H_3O^+ \qquad (5)$$

$$DGA + CO_2 + H_2O \leftrightarrow DGACOO^- + H_3O^+ \qquad (6)$$

$$DGAH^+ + H_2O \leftrightarrow DGA + H_3O^+ \qquad (7)$$

The total amount of water, carbon dioxide, MOR, and DGA present in the liquid phase are specified. Equilibrium is first calculated in the liquid phase, and then vapor/liquid equilibrium is calculated for all molecular species (MOR, DGA, $H_2O$, $CO_2$).

Gas-phase nonidealities are calculated using the Soave−Redlich−Kwong (SRK) equation of state.[15] Liquid-phase nonidealities are calculated using the electrolyte NRTL model.[16−19] The use of the electrolyte NRTL model in amine/acid gas systems has been described previously by Austgen,[2] Posey,[3] and Bishnoi and Rochelle.[7] This work most closely resembles that of Bishnoi and Rochelle[7] with $CO_2$ referenced to infinite dilution in water. All ions are also referenced to infinite dilution in water. The MOR, DGA, and $H_2O$ are all referenced to the respective pure components at the system temperature. The reader is referred to Bishnoi and Rochelle[7] for more detailed description of the gas and liquid-phase models used to account for nonideality.

$\tau$ parameters are defined in order to be consistent with the work of Bishnoi and Rochelle.[7] $\tau$ parameters for molecule/molecule interactions are defined as

$$\tau = A + \frac{B/K}{T/K} \qquad (8)$$

$\tau$ parameters for salt pair/molecule and molecule/salt pair are defined with $T_{ave}$ as 353.15 K:

$$\tau = A + B/K\left(\frac{1}{T/K} - \frac{1}{T_{ave}/K}\right) \qquad (9)$$

Default parameters consistent with Aspen Plus version 8.5 were used in this work. This is consistent with the work of Austgen,[2] Posey,[3] and Bishnoi and Rochelle.[7] Critical constants used by the SRK equation of state and the accentric factor were taken from the Design Institute for Physical Properties (DIPPR) database.[20] Brevli−O'Connell parameters (Table 1) used in this work were obtained from the original work.[21]

**Table 2. . Values for $CO_2$ Henry's Constant and NRTL Parameters (Regressed from $N_2O$ solubility data for MOR and DGA)[12]**

| $\ln(H_x/(\text{Pa/mol fraction})) = A + B/(T/K) + C\ln(T/K) + D(T/K)$ | |
|---|---|
| A | 170.7 |
| B | −8477 |
| C | −22.0 |
| D | 3.33E−03 ± 8.3E−05 |

| molecule pair[a] | $A$ | $B$ |
|---|---|---|
| $CO_2$-MOR | 0.0 | 0.0 |
| MOR−$CO_2$ | −1.95 ± 0.4921 | 0.0 |
| $CO_2$-DGA | 0.0 | 0.0 |
| DGA-$CO_2$ | −1.98 ± 0.18 | 0.0 |

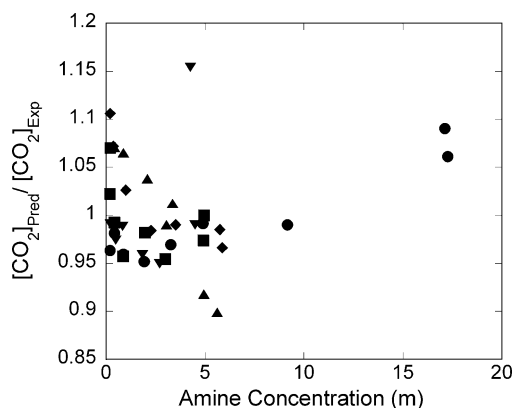[a] Parameters without a standard deviation were not regressed.



**Figure 1.** Results of $N_2O$ data regression in unloaded aqueous solutions of MOR and DGA[12]: ●, DGA, 298 K; ■, DGA, 303 K; ◆, DGA, 318 K; ▲, DGA, 333 K; ▼, MOR, 303 K.

Critical compressibilities used in the Rackett model were obtained from the DIPPR database. The dielectric constant of MOR was assumed to be the same as MEA. The Antoine equation for MOR was obtained from Stephenson and Malanowski.[22]

Versteeg and Van Swaaij[12] measured the solubility of $N_2O$ in aqueous DGA and MOR and estimated from these data the solubility of unreacted $CO_2$. The Henry's law constant and the interaction parameters of DGA + $CO_2$ and MOR + $CO_2$ were adjusted simultaneously using these data for DGA and MOR[12] so that $CO_2$ solubility decreases with increasing amine concentration. The regression results are given in Table 2 and Figure 1. The Henry's constant is the thermodynamic value with the reference state for $CO_2$ at infinite dilution in water that best represents the full set of data.

Equilibrium constants for reactions 1, 2, 3, 4, and 7 are documented in Table 3 along with their sources. The first and second dissociation constants of $CO_2$, the DGA protonation, and the water dissociation constants are unchanged from the work of Austgen.[2] The dissociation equilibrium constant for MOR is reported in Vistad et al.[23] and is based on molality scale. It is modified in this work in order to treat MOR as a solvent rather than as a solute and also to change the equilibrium constant from the molality scale to the mole fraction scale. This will be discussed later.

## Solubility of Carbon Dioxide

Data for $CO_2$ solubility in 3.5 m MOR, 17.7 m DGA, and 3.6 m MOR + 14.7 m DGA at (298, 313, and 333) K are given in Table 4. Throughout this work, loading is represented as mol $CO_2$/mol amine where amine includes DGA plus MOR. We chose to work with 3.6 m MOR + 14.7 m DGA (17 % of the total DGA concentration) since the lean amine concentration

**Table 3. Temperature Dependence of Equilibrium Constants, Mole Fraction Based**

| eq no. | equilibrium constant | A | B | C | D | value at 313 K | reference |
|---|---|---|---|---|---|---|---|
| 1 | $\dfrac{a_{HCO_3^-}a_{H_3O^+}}{a_{CO_2}a_{H_2O}^2}$ | 231.4 | −12092 | −36.78 | 0.0 | 8.55E−9 | 3 |
| 2 | $\dfrac{a_{H_3O^+}a_{CO_3^-}}{a_{HCO_3^-}a_{H_2O}}$ | 216.0 | −12432 | −35.48 | 0.0 | 1.04E−12 | 3 |
| 3 | $\dfrac{a_{H_3O^+}a_{OH^-}}{a_{H_2O}^2}$ | 132.9 | −13446 | −22.48 | 0.0 | 9.15E−18 | 3 |
| 4 | $\dfrac{a_{MOR}a_{H_3O^+}}{a_{H_2O}a_{MORH^+}}$ | −4.53 | −6296 | 0.0 | 0.0 | 1.98E−11 | 23 |
| 5 | $\dfrac{a_{MORCOO^-}a_{H_3O^+}}{a_{MOR}a_{CO_2}a_{H_2O}}$ | −24.9 | 5141 | 0.0 | 0.0 | −8.5 | this work |
| 6 | $\dfrac{a_{DGACOO^-}a_{H_3O^+}}{a_{DGA}a_{CO_2}a_{H_2O}}$ | −36.0 | −825 | 0.0 | 0.0 | −10.5 | this work |
| 7 | $\dfrac{a_{DGA}a_{H_3O^+}}{a_{H_2O}a_{DGAH^+}}$ | 1.70 | −8432 | 0.0 | −0.504E−2 | 2.25E−12 | 2 |

*a* $\ln (K_x) = A + B/(T/K) + C \ln(T/K) + D(T/K)$.

**Table 4. CO$_2$ Solubility**

| 17.7 m DGA | | | 3.5 m MOR | | | 3.6 m MOR+14.7 m DGA | | |
|---|---|---|---|---|---|---|---|---|
| $T$ | loading mol CO$_2$ | $P^*_{CO_2}$ | $T$ | loading mol CO$_2$ | $P^*_{CO_2}$ | $T$ | loading mol CO$_2$ | $P^*_{CO_2}$ |
| K | mol DGA | Pa | K | mol MOR | Pa | K | mol amine | Pa |
| 297.2 | 0.23 | 15 | 297.4 | 0.08 | 10 | 298.7 | 0.13 | 5 |
| 296.8 | 0.43 | 735 | 312.8 | 0.08 | 35 | 313.7 | 0.13 | 20 |
| 314.2 | 0.10 | 10 | 333 | 0.08 | 250 | 331.7 | 0.13 | 515 |
| 312.5 | 0.23 | 75 | 312.8 | 0.21 | 1175 | 297.7 | 0.27 | 25 |
| 311.9 | 0.42 | 2120 | 332.5 | 0.21 | 6150 | 313.8 | 0.27 | 285 |
| 331.5 | 0.11 | 145 | 297 | 0.32 | 9540 | 334.7 | 0.27 | 1180 |
| 333.2 | 0.24 | 795 | 313.1 | 0.32 | 53700 | 297.7 | 0.36 | 150 |
| 332.6 | 0.42 | 14750 | | | | 313.2 | 0.36 | 725 |
| | | | | | | 331.1 | 0.36 | 6700 |
| | | | | | | 298.2 | 0.45 | 3775 |
| | | | | | | 314.4 | 0.45 | 16190 |

**Table 5. Heat of Absorption of CO$_2$ at Various Loadings for 3.5 m MOR, 17.7 m DGA, and 3.6 m MOR + 14.7 m DGA***a*

| solvent | CO$_2$ loading | heat of absorption |
|---|---|---|
| m | (mol/mol amine) | kJ·mol$^{-1}$ |
| 3.5 MOR | 0.08 | 79.9 |
| 3.5 MOR | 0.21 | 72.4 |
| 3.5 MOR | 0.32 | 82.4 |
| 17.7 DGA | 0.10 | 144.8 |
| 17.7 DGA | 0.23 | 92.5 |
| 17.7 DGA | 0.42 | 76.6 |
| 3.6 MOR+14.7 DGA | 0.13 | 121.8 |
| 3.6 MOR+14.7 DGA | 0.26 | 87.4 |
| 3.6 MOR+14.7 DGA | 0.35 | 93.3 |
| 3.6 MOR+14.7 DGA | 0.45 | 70.3 |

*a* Calculated from experimental data.

of MOR at Saudi Aramco gas plants at the beginning of this problem had reached > 10 % in several trains and > 14 % in one. The current MOR concentration in the lean DGA is 5−6 wt % after several process changes.[24]

The replacement of DGA with 3.6 m (11 wt %) MOR increases the vapor pressure of CO$_2$ by a factor of 5 to 7 at high loading. The data of DGA + MOR converges with the equilibrium partial pressure of DGA at CO$_2$ loading below 0.2. Martin et al.[10] obtained solubility data for CO$_2$ in 14.3 m (60 wt %) DGA at (323 and 373) K for regions of high acid gas partial pressures. Dingman et al.[11] obtained a large amount of data in solutions of 17.7 m DGA down to low acid gas loading.

These other CO$_2$ solubility data complement the data taken in this work.

The heat of CO$_2$ absorption ($\Delta H_{abs}$) in 3.5 m MOR, 17.7 m DGA, and 3.6 m MOR + 14.7 m DGA was determined directly at specific values of CO$_2$ loading using the VLE data in Table 4 from (298 to 333) K. With the Clayperon equation,[25] $\Delta H_{abs}$ can be calculated as

$$\frac{d(\ln(P_{CO_2}^*/Pa))}{d(1/(T/K))} = -\frac{\Delta H_{abs}/kJ \cdot mol^{-1}}{0.008314 \; kJ \cdot mol^{-1} \cdot K^{-1}} \quad (10)$$

The results are given in Table 5.

## $^{13}$C NMR

In a rich solution of primary or secondary amine, the concentration of unreacted amine (RNH$_2$) and bicarbonate (HCO$_3^-$) depends on the carbamate stability constant ($K_{carb}$):

$$R_2NH + HCO_3^- \xleftrightarrow{K_{carb}} RNHCOO^- + H_2O \quad (11)$$

$$K_{carb} = \frac{[R_2NH-CO_2^-]}{[HCO_3^-][R_2NH]} \quad (12)$$

The solution speciation in aqueous 3.5 m MOR, 17.7 m DGA, and 3.6 m MOR + 14.7 m DGA was measured by $^{13}$C NMR at (300, 313, and 333) K and at $^{13}$CO$_2$ loading from 0 to 0.5 mol
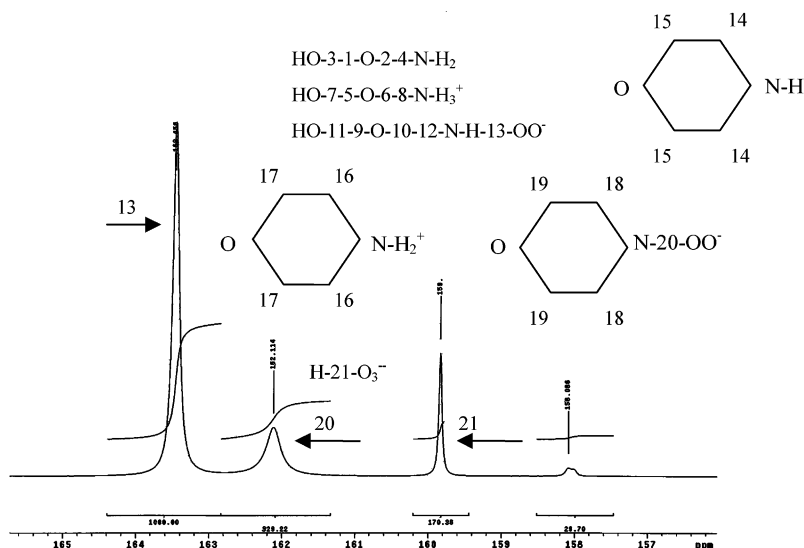
**Figure 2.** $^{13}C$ NMR spectrum of 3.6 m MOR + 14.7 m DGA at 300 K and 0.52 mol $^{13}CO_2$/mol amine, $\delta$ (ppm) = 157 to 165.
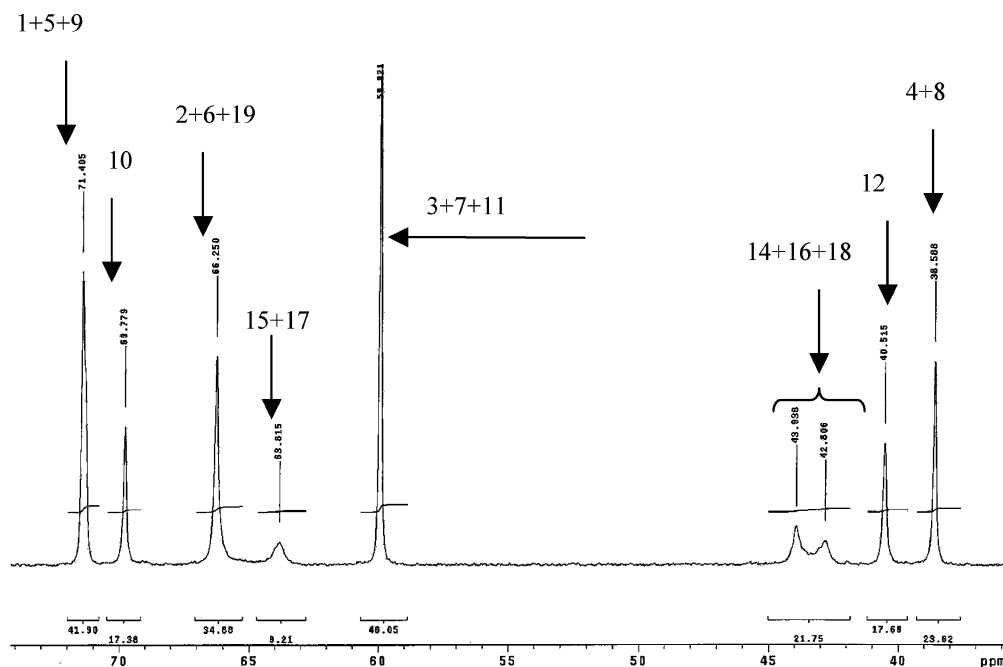


**Figure 3.** $^{13}C$ NMR spectrum of 3.6 m MOR + 14.7 m DGA at 300 K and 0.52 mol $^{13}CO_2$/mol amine, $\delta$ (ppm) = 36 to 74.

**Table 6. . Detailed $^{13}C$ NMR Results for 3.6 m MOR + 14.7 m DGA at 300 K and 0.52 mol $^{13}CO_2$/mol Amine**

| carbon no. | $\delta$ (ppm) | area |
|---|---|---|
| 4 & 8 | 38.6 | 23.62 |
| 12 | 40.5 | 17.69 |
| 14, 16, & 18 | 43.9, 42.8, & 40.5 | 21.75 |
| 3, 7, & 11 | 59.9 | 46.05 |
| 15 &17 | 63.9 | 9.21 |
| 2, 6, &19 | 66.2 | 34.88 |
| 10 | 69.8 | 17.38 |
| 1, 5, & 9 | 71.4 | 41.90 |
| 21 | 158.8 | 170.38 |
| 13 | 162.1 | 329.22 |
| 20 | 163.5 | 1000.00 |

**Table 7. $^{13}C$ NMR in 17.7 m DGA**

| T/K | loading | DGACOO⁻/HCO₃⁻ [a] | $K_{carb}$/M⁻¹ [b] |
|---|---|---|---|
| 300 | 0.167 | 193.1 | 56.5 |
| 333 | 0.179 | 78.7 | 25.0 |
| 300 | 0.337 | 102.4 | 61.2 |
| 333 | 0.326 | 42.9 | 25.0 |
| 300 | 0.362 | 59.5 | 38.5 |
| 313 | 0.384 | 52.9 | 37.8 |
| 333 | 0.382 | 32.6 | 22.2 |
| 300 | 0.468 | 6.6 | 63.1 |
| 313 | 0.481 | 6.1 | 39.3 |
| 333 | 0.475 | 5.8 | 25.5 |

[a] Ratio of peak areas in the $^{13}C$ NMR spectrum. [b] $K_{carb} = C_{AMCOO^-}/C_{AM}C_{HCO_3^-}$, where $C_i$ is the concentration of species $i$ in mol/L.

$^{13}CO_2$/mol amine. Figures 2 and 3 show typical $^{13}C$ NMR spectra for 3.6 m MOR + 14.7 m DGA. Table 6 gives the detailed NMR results of the spectra in Figures 2 and 3. Tables 7, 8, and 9 also give the ratio of carbamate to bicarbonate peak areas as a function of CO₂ loading and temperature for all the $^{13}C$ NMR spectra acquired in this work. All NMR spectra from this work can be found in Al-Juaied.[26]

The peaks were identified by comparing spectra of solutions with MOR or DGA alone with and without added $^{13}CO_2$. The chemical shifts of specific peaks were practically identical in all solutions. For chemical shifts of 37 to 74 ppm, carbon peaks of protonated/free amine (AMH⁺ + AM) were observed; hence, the remaining peaks could be identified with the carbamate form

**Table 8. $^{13}C$ NMR in 3.5 m MOR**

| $T/K$ | loading | MORCOO$^-$/HCO$_3^{-\,a}$ | $K_{carb}$/M$^{-1\,b}$ |
|---|---|---|---|
| 300 | 0.478 | 2.76 | 6.8 |
| 313 | 0.478 | 1.87 | 3.8 |
| 333 | 0.478 | 1.51 | 2.8 |
| 300 | 0.405 | 4.57 | 6.9 |
| 313 | 0.392 | 3.12 | 4.1 |
| 333 | 0.392 | 1.79 | 2.1 |
| 300 | 0.370 | 3.75 | 4.4 |
| 313 | 0.370 | 2.76 | 3.1 |
| 333 | 0.370 | 1.72 | 1.8 |
| 300 | 0.569 | 1.46 | 7.2 |
| 313 | 0.569 | 1.18 | 4.5 |
| 333 | 0.569 | 1.24 | 5.0 |
| 300 | 0.428 | 4.60 | 8.3 |
| 313 | 0.428 | 3.37 | 5.7 |
| 333 | 0.428 | 2.62 | 4.1 |
| 300 | 0.325 | 10.9 | 11.0 |
| 313 | 0.325 | 8.01 | 8.0 |
| 333 | 0.325 | 4.77 | 4.6 |
| 300 | 0.258 | 16.7 | 12.6 |
| 313 | 0.258 | 11.6 | 8.7 |
| 333 | 0.258 | 6.31 | 4.7 |

$^a$ Ratio of peak areas in the $^{13}C$ NMR spectrum. $^b$ $K_{carb} = C_{AMCOO^-}/C_{AM}C_{HCO_3^-}$, where $C_i$ is the concentration of species $i$ in mol/L.

**Table 9. $^{13}C$ NMR in 3.6 m MOR/14.7 m DGA**

| $T/K$ | loading | (DGACOO$^-$ + MORCOO$^-$)/HCO$_3^{-\,a}$ |
|---|---|---|
| 300 | 0.524 | 7.80 |
| 313 | 0.524 | 7.18 |
| 333 | 0.524 | 6.50 |
| 300 | 0.364 | 54.74 |
| 313 | 0.374 | 37.67 |
| 333 | 0.374 | 24.00 |
| 300 | 0.271 | 127.1 |
| 313 | 0.285 | 73.00 |
| 333 | 0.285 | 52.11 |

$^a$ Ratio of peak areas in the $^{13}C$ NMR spectrum.

**Table 10. Comparison of Carbamate Stability Constants (Molarity Based), Equation 12**

| amine | $T/K$ | reference | $K_{carb}$/M$^{-1}$ |
|---|---|---|---|
| MOR | 283 | 28 | 8 |
| | 300 | this work | 8.2 |
| | 313 | this work | 5.4 |
| | 333 | this work | 3.6 |
| DGA | 298 | 2 | 12 |
| | 300 | this work | 61.0 |
| | 313 | this work | 38.6 |
| | 333 | this work | 24.4 |

of the amines (AMCO$_2^-$). The peaks observed at chemical shifts of 37 to 74 ppm are those associated with natural $^{13}C$ in the protonated/free amine/carbamate anion backbone carbons (AMH$^+$, AM, AMCO$_2^-$). The carbon peaks of carbamate anion (AM$^{13}$CO$_2^-$) and bicarbonate ion (H$^{13}$CO$_3^-$) appeared at 159 to 165 ppm. Those carbons are associated with $^{13}$CO$_2$. Bicarbonate ions in CO$_2$ + MOR + H$_2$O, CO$_2$ + DGA + H$_2$O, and CO$_2$ + MOR + DGA + H$_2$O showed similar chemical shifts at the same carbon dioxide absorbing conditions. The quantitative analysis of bicarbonate ion (H$^{13}$CO$_3^-$) was made by considering the ratio of the peak areas of the carbons in the carbamate form of the amine and the carbons in the carbamate anion peak areas. The CO$_2$ loading can also be determined from the peak areas of protonated/free amine, bicarbonate ion, and carbamate anion peak areas. It should be noted that the peak area of the carbon attached to nitrogen and the four methylene carbons of the carbamate have different intensities. In this work, it was assumed that the formation of carbonate ions is not likely to occur because the pH of the amine solutions was low enough (pH of 7 to 10) to guarantee that the carbonate–bicarbonate
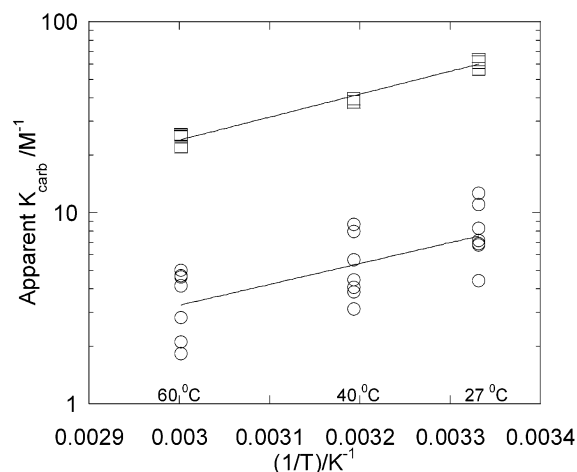
**Figure 4.** Carbamate stability constant arrhenius fit. The symbols represent the observations; $\bigcirc$, 3.5 m MOR; $\square$, 17.7 m DGA. The lines are curve fit.

**Table 11. Excess Heat of Mixing at Infinite Dilution in Water and 25 °C**

| species$^a$ | $H_{AM}^{EX,\infty}$/kJ·mol$^{-1}$ | reference |
|---|---|---|
| piperazine$^b$ | −59 | Dortmund modified UNIFAC |
| piperazine | −38 | 30 |
| piperazine | −26 | 31 |
| morpholine | −25 | 31 |
| cyclohexylamine | −23 | 31 |

$^a$ All species listed are liquids in their pure state at ambient conditions except PZ. $^b$ Reference state of most components in Dortmund UNIFAC database is liquid.

equilibrium is shifted more toward the bicarbonate side at various CO$_2$ loadings. Figures 2 and 3 give the detailed identification of the peaks.

Table 10 is a summary of the apparent carbamate stability constants obtained in the present study. As defined by eq 12, the apparent constant is based on concentrations (molarity), not activities, and does not include a water concentration. Literature values of the apparent carbamate stability constants of MOR and DGA are also listed as a reference. It is clear that the carbamate stability constant in 17.7 m aqueous DGA is greater than that of MOR. This observation is consistent with the p$K_a$ values at 298 K of DGA, 9.46, and MOR, 8.70.[27]

Figure 4 gives the apparent carbamate stability constant as a function of temperature. The temperature dependence is equivalent to a heat of reaction of 22.9 kJ·mol$^{-1}$ for DGA and 20.9 kJ·mol$^{-1}$ for MOR. Again this result shows that MOR requires less heat of reaction to regenerate compared to DGA since it forms less stable carbamate.

## Activity of Diglycolamine and Morpholine in Aqueous Mixtures

Wu et al.[29] have measured vapor liquid equilibrium for MOR/H$_2$O at (348 and 368) K. Analysis of activity coefficients yields an excess heat of mixing at infinite dilution of −16.7 kJ·mol$^{-1}$ for liquid MOR:

$$\ln\left(\frac{\gamma^{(2)}MOR}{\gamma^{(1)}MOR}\right)_{P,x} = \frac{H_2^{Ex}/kJ\cdot mol^{-1}}{0.008314\ kJ\cdot mol^{-1}\cdot K^{-1}}\left[\frac{1}{T^{(2)}/K} - \frac{1}{T^{(1)}/K}\right] \quad (13)$$

A comparison of the excess heat of mixing of different amines at infinite dilution is provided in Table 11. The values for amines are consistently negative and seem to be related to the amino

group. The value of $-16.7$ kJ·mol$^{-1}$ for MOR is lower than the standard value of $-25$ kJ·mol$^{-1}$ at 298 K. The former value is obtained by extrapolation from the high-temperature data as shown in eq 13.

As noted previously, MOR is referenced to the pure component at the system temperature:

$$\gamma_{MOR} \rightarrow 1 \text{ as } x_{MOR} \rightarrow 1 \tag{14}$$

Using the following equation[2] to relate $K_x'$ and $K_x$;

$$K_x' = K_x \gamma_{MOR}^{\infty} \tag{15}$$

where $\gamma_{MOR}^{\infty}$ is the symmetrically normalized activity coefficient of MOR at infinite dilution in water, $K_x$ is the dissociation constant expressed on the mole fraction, and $K_x'$ is the new dissociation constant after adopting the above normalization convention.

Vistad et al.[23] determined the dissociation constant of MOR as a function of temperature by potentiometric pH measurement of a MOR−H$_2$O solution (2.1:60 ratio) while varying the temperature within the range (273 to 323) K. The determined temperature dependence of p$K_a$ is the following:

$$pK_a = \frac{1560}{T/K} + 3.52 \tag{16}$$

The above dissociation constant is reported on the molality scale. The p$K_a$ is the negative logarithm (base 10) of $K_m$ and can be converted to $K_x$ using the following equation[2]:

$$\ln K_x = \ln K_m - \ln\left(\frac{1000}{M_s}\right) \tag{17}$$

where $M_s$ is the molecular weight of water. Therefore, $\ln K_x$ is given by

$$\ln K_x = -12.1 - \frac{3592}{T/K} \tag{18}$$

The NRTL parameters for MOR/H$_2$O and H$_2$O/MOR were then adjusted to fit the VLE data of MOR/H$_2$O and the excess heat of reaction at 298 K. The results of the regression are shown in Figure 5 and Table 12. Using the following equation[2] for $\gamma_{MOR}^{\infty}$:

$$\ln \gamma_{MOR}^{\infty} = \tau_{H_2O-MOR} + G_{MOR-H_2O}\tau_{MOR-H_2O} \tag{19a}$$

$$\tau_{H_2O-MOR} = A_{H_2O-MOR} + \frac{B_{H_2O-MOR}/K}{T/K} \tag{19b}$$

$$\tau_{MOR-H_2O} = A_{MOR-H_2O} + \frac{B_{MOR-H_2O}/K}{T/K} \tag{19c}$$

$$G_{MOR-H_2O} = \exp[-0.2\tau_{MOR-H_2O}] \tag{19d}$$

and the NRTL parameters for MOR/H$_2$O and H$_2$O/MOR in Table 12, $\gamma_{MOR}^{\infty}$ can be converted into the common temperature form used for the equilibrium constants:

$$\ln \gamma_{MOR}^{\infty} = 7.59 - \frac{2704}{T/K} \tag{20}$$

Accurate prediction of the MOR activity coefficient is useful in two ways. It helps predict the volatility and losses of the amine as well as correcting the equilibria that involve MOR for the effect of DGA. From Equations 15, 18, and 20, the
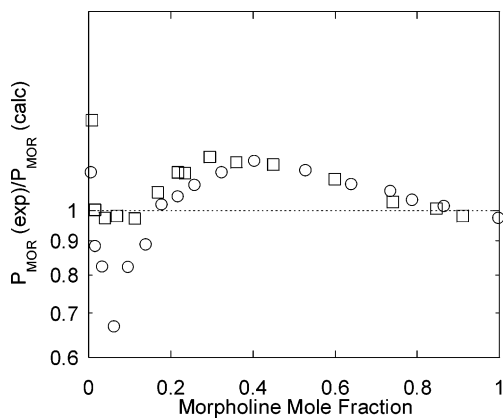


**Figure 5.** Results of regression of the equilibrium partial pressure of MOR in MOR−H$_2$O mixture. Fitting $H^E$ = d ln $\gamma_{MOR}^{\infty}$/d(1/$T$) at 298 K to $-25$ kJ/mol; ○, 348 K; □, 368 K.

**Table 12. Values of NRTL Binary Interaction Parameters for MOR−H$_2$O (fitted) and DGA−H$_2$O[2]**

| molecule pair | A | B/K |
|---|---|---|
| H$_2$O−MOR | $4.62 \pm 0.23$ | $0.00^a$ |
| MOR−H$_2$O | $0.000^a$ | $-960 \pm 1.65$ |
| DGA−H$_2$O | $1.99 \pm 0.35$ | $0.00$ |
| H$_2$O−DGA | $0.000$ | $-770 \pm 62.2$ |

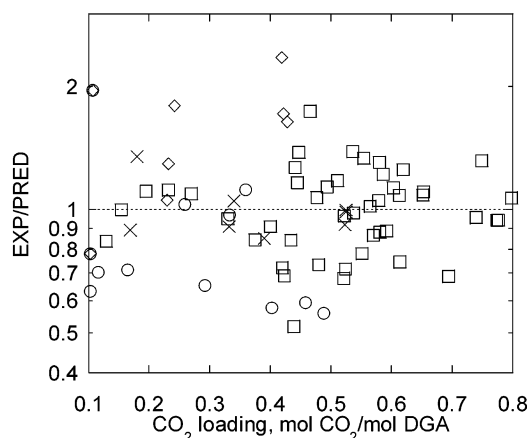$^a$ Parameters fixed at zero could not be estimated with statistical significance.



**Figure 6.** Results of VLE and $^{13}$C NMR data regression of DGA: ○, 17.7 m DGA, Dingman et al.;[11] □, 14.3 m DGA, Martin et al.;[10] ◇, this work, $P_{CO_2}^*$; ×, this work, DGACOO$^-$/HCO$_3^-$.

protonation equilibrium constant (mole fraction based) for MOR is given by

$$\ln K_x' = -4.53 - \frac{6296}{T/K} \tag{21}$$

## Parameter Regression Results of CO$_2$ Solubility and $^{13}$C NMR Data

*DGA−CO$_2$.* The electrolyte−NRTL parameters and the carbamate equilibrium constant for the DGA−CO$_2$ system were regressed to two VLE data sets and VLE and the NMR data set from this work. The four data sets were simultaneously regressed, and the resulting parameters are given in Table 13. In this work, only the partial pressure for the VLE data and the ratio of the carbamate to the bicarbonate mole fractions for the NMR data were adjusted. As can be seen from Figure 6, the ratios of experimental to calculated are well-distributed about a value of unity. In general, the model appears to represent the

**Table 13. Non-Default Parameters for the NRTL Model**

| parameter | $A$ | $B$ | $\tau_{313}$ | default $\tau$ |
|---|---|---|---|---|
| $\tau$ (IH$_2$O, IDGAH, IHCO$_3$) | 5.9 ± 0.49 | 5905 ± 901 | 8.0 | 8 |
| $\tau$ (IH$_2$O, IDGAH, IDGACOO) | 7.5 ± 0.32 | 0.00 | 7.5 | 8 |
| $\tau$ (IDGAH, IHCO$_3$, IH$_2$O) | −4.0 | 0.00 | −4.0 | −4 |
| $\tau$ (IDGAH, IDGACOO, IH$_2$O) | −4.0 | −1222 ± 93 | −4.4 | −4 |
| $\tau$ (IDGAH, IDGACOO, IDGA) | −6.7 ± 0.27 | 0.00 | −6.7 | −8.0 |
| ln $K_x$ DGA carbamate | −36.0 ± 0.40 | 825[a] | | |
| $\tau$ (IH$_2$O, IMORH, IHCO$_3$) | 20.4 ± 0.42 | −20133[a] | 13.1 | 8 |
| $\tau$ (IH$_2$O, IMORH, IMORCOO) | 10.2 ± 1.21 | −11568[a] | 6.0 | 8 |
| $\tau$ (IMORH, IHCO$_3$, IH$_2$O) | −8.54[a] | 7345 ± 965 | −5.9 | −4 |
| $\tau$ (IMORH, IMORCOO, IH$_2$O) | −6.99[a] | 2402 ± 586 | −6.1 | −4 |
| $\tau$ (IMORH, IMORCOO, IMOR) | −5.74 ± 0.75 | 0.00 | −5.7 | −8.0 |
| ln $K_x$ MOR carbamate | −14.2[a] | 1545 ± 306 | | |
| $\tau$ (IH$_2$O, IMORH, IDGACOO) | 4.9 ± 1.4 | 0.00 | 4.9 | 8 |
| $\tau$ (IMORH, IDGACOO, IH$_2$O) | −8.5 ± 0.21 | 4164 ± 1245 | −7.0 | −4 |
| $\tau$ (IDGAH, IMORCOO, IH$_2$O) | −5.0 ± 0.18 | 602 ± 550 | −4.8 | −4 |

[a] $\tau = A + B/K[1/(T/K) - 1/(T_{ave}/K)]$ for salt pair/molecule and molecule/salt pair. ln $K = A + (B/K)/(T/K)$.
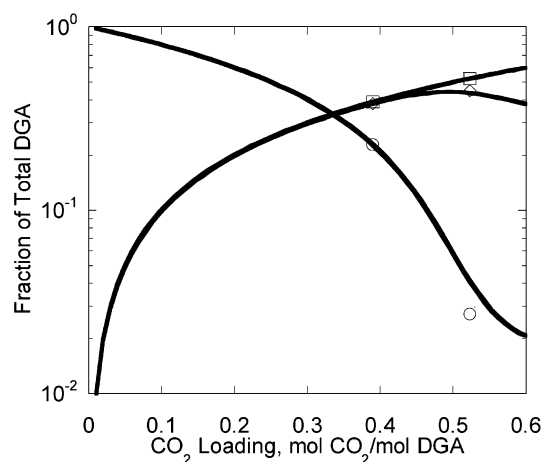


**Figure 7.** Results of regression of $^{13}$C NMR data in 17.7 m DGA system at 313 K. The symbols represent the observations: ○, DGA; □, DGAH$^+$; ◇, DGACOO$^-$. The lines represent the NRTL model prediction using parameters from Table 13.
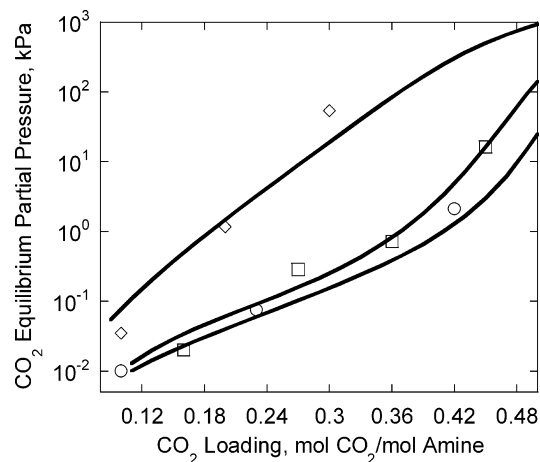


**Figure 8.** CO$_2$ partial pressure as a function of loading at 313 K. The symbols represent the observations: ○, 17.7 m DGA; □, 3.6 m MOR/14.7 m DGA; ◇, 3.5 m MOR. The lines represent the NRTL model prediction using parameters from Table 13.
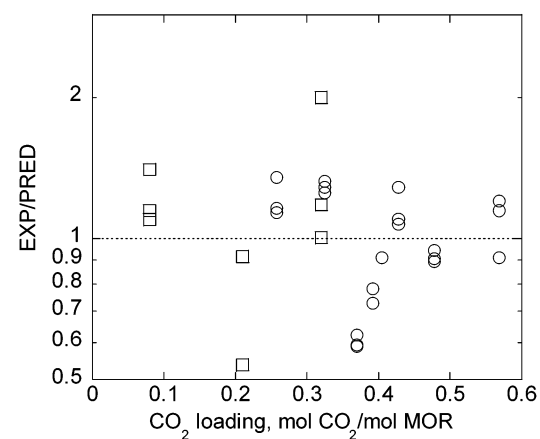
experimental data even as it varies over extremely wide ranges of CO$_2$ pressure and loading.

Most of the parameters are well predicted as indicated by the low standard deviation. The regressed $\tau$ value obtained in this work does not deviate far from the default value. This places some confidence in their absolute value. Figure 7 gives the predicted speciation at 313 K. Figure 8 compares partial pressure predictions from the current model to the VLE data obtained in this work for 17.7 m DGA at 313 K.

***MOR−CO$_2$.*** The electrolyte−NRTL parameters and the carbamate equilibrium constant for the MOR−CO$_2$ system were regressed to the VLE and $^{13}$C NMR data. The two data sets were simultaneously regressed. The parity plot and resulting parameters are given in Figure 9 and Table 13.

The regressed $\tau$ values obtained in this work do not deviate far from the default values as can be seen in Table 13. Figure 10 gives the predicted speciation at 313 K. Figure 8 compares partial pressure predictions from the current model to the VLE data obtained in this work for 3.5 m MOR at 313 K. The CO$_2$ vapor pressure in 3.5 m MOR is greater than in 17.7 m DGA, consistent with the observation of less stable MOR carbamate as compared to the more stable DGA carbamate.

***MOR−DGA−CO$_2$.*** The parameters obtained in the single amine systems were used in the MOR−DGA−CO$_2$ system. Similarities can be seen in the two amine tau values. The VLE and $^{13}$C NMR data sets for the 3.6 m MOR + 14.7 m DGA



**Figure 9.** Results of VLE and NMR data regression of the MOR−CO$_2$ system fixing CO$_2$ solubility to the N$_2$O analogy: ○, MORCOO$^-$/HCO$_3^-$; □, $P^*_{CO_2}$.

were simultaneously regressed. The parity plot and the resulting parameters are given in Figure 11 and Table 13.

Parameters for the water mixed amine interactions were regressed. Table 13 lists the parameter values that have been used to represent interaction in the DGA + MOR systems. Figure 12 gives the $^{13}$C NMR predicted speciation at 313 K. Figure 8 compares partial pressure predictions from the current model to the VLE data obtained in this work for 3.6 m MOR + 14.7 m DGA at 313 K. Figure 13 compares predictions of
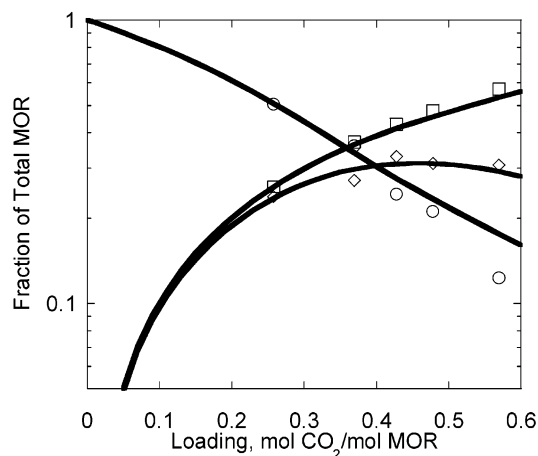
**Figure 10.** Results of regression of $^{13}C$ NMR data in the 3.5 m MOR system at 313 K. The symbols represent the observations: ○, MOR; □, MORH$^+$; ◇, MORCOO$^-$. The lines represent the NRTL model prediction using parameters from Table 13.
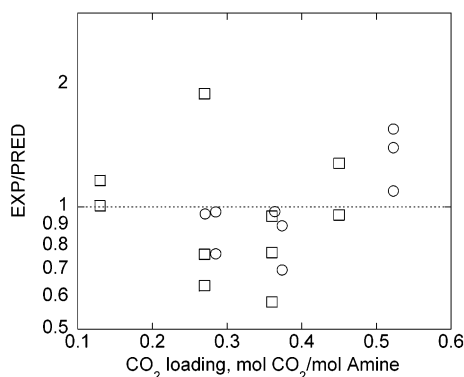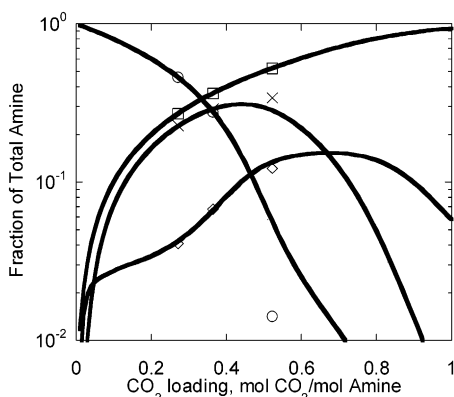


**Figure 11.** Results of VLE and NMR data regression of the MOR−DGA−CO$_2$ system. Fixing CO$_2$ solubility to the N$_2$O Analogy: ○, (MORCOO$^-$ + DGACOO$^-$)/HCO$_3$$^-$; □, $P^*_{CO_2}$.



**Figure 12.** Results of regression of $^{13}C$ NMR data in 3.6 m MOR + 14.7 m DGA system at 313 K. The symbols represent the observations; ○, MOR + DGA; □, MORH$^+$ + DGAH$^+$; ◇, MORCOO$^-$; ×, DGACOO$^-$. The lines represent the NRTL model prediction using parameters from Table 13.

the current model for (298, 313, and 333) K in 13.7 m DGA and 3.6 m MOR + 14.7 m DGA.

## Solvent Working Capacity

At a typical natural gas plant, the gas feed contains 10.3 % CO$_2$ and is contacted with 17.7 m solvent DGA in an absorber at a total pressure of 1500 kPa and (313 to 333) K. The corresponding CO$_2$ partial pressure is 155 kPa. To achieve
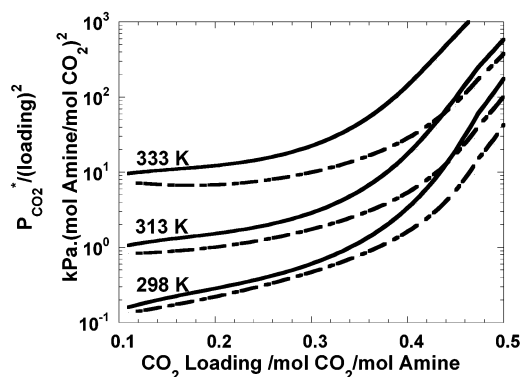


**Figure 13.** Calculated CO$_2$ equilibrium partial pressure for 17.7 m DGA (dashed lines) and 3.6 m MOR + 14.7 m DGA (solid lines).

**Table 14. Comparison of Working Capacities at 333 K, $P_{CO_2,rich}$ = 155 kPa, and $P_{CO_2,lean}$ = $10^{-2}$ kPa**

| solvent | lean loading (mol/mol) | rich loading (mol/mol) | working capacity (mol/mol) |
|---|---|---|---|
| 17.7 m DGA | ∼0.11 | 0.51 | 0.40 |
| 3.6 m MOR/14.7 m DGA | ∼0.12 | 0.46 | 0.33 |

maximum capacity of each volume of solution circulated, the circulation rate is set so that the maximum recommended loading can be achieved. Typically the maximum loading is represented as an approach to equilibrium set by the VLE data. Assuming that the approach to equilibrium at the bottom of the absorber is 70 % and the equilibrium partial pressure of CO$_2$ under regeneration conditions is $10^{-2}$ kPa, the solvent working capacity can then be determined. As can be seen in Figure 8, the blend solution shows steeper slope compared to the 17.7 m DGA. The 17.7 m DGA provides the highest equilibrium loading compared to blend mixture. At 333 K, the 3.6 m MOR reduces the working capacity by 17 % as compared to the 17.7 m DGA working capacity. In terms of solvent capacity, 17.7 m DGA is better than 3.6 m MOR/14.7 m DGA because it requires a lower solvent circulation rate. Table 14 gives the results of the calculations at 333 K.

## Regeneration Energy Requirements

The main source of energy consumption in an amine process is the regeneration step. The total energy required to regenerate a CO$_2$ loaded solvent can be expressed as follows:

total energy = heat of reaction + sensible heat + latent heat of vaporization of water

In the regeneration step, the rich solvent temperature must be raised to the stripper bottom temperature by sensible heat transfer. The amount of heat required for this process is dictated by the specific heat capacity of the solvent, which should not vary much between DGA and MOR. In addition, the water component of the solvent must also be vaporized to generate the stripping vapor. This requirement will depend on the approach to CO$_2$ saturation and should not vary significantly from DGA to the blend.

Finally, sufficient heat must be provided to break up the CO$_2$−solvent complex formed during the absorption process. This can be accounted for by the heat of reaction. The heat of reaction ($\Delta H_{abs}$) of 17.7 m DGA and 3.6 m MOR + 14.7 m DGA solutions was determined at various loadings at 333 K. Using the Clapeyron equation (eq 10), the $\Delta H_{abs}$ can be determined. Results are displayed graphically in Figure 14. Note that loading has a significant effect on the heat of absorption:
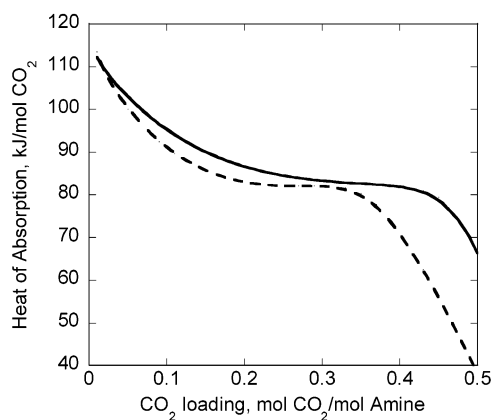
**Figure 14.** Heat of $CO_2$ absorption at 333 K predicted by the regressed thermodynamic model. Solid line represents 17.7 m DGA, and dashed line represents 3.6 m MOR + 14.7 m DGA.
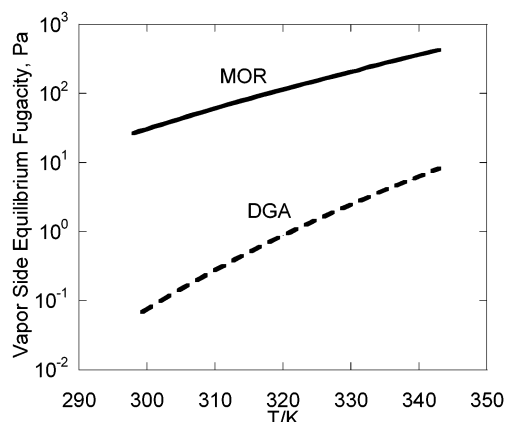


**Figure 15.** Vapor pressure of MOR and DGA over 3.6 m MOR/14.7 m DGA and $CO_2$ loading of 0.01 mol $CO_2$/mol amine predicted by the regressed thermodynamic model. Solid line represents MOR, and dashed line represents DGA.

increasing the loading decreases the heat of absorption. As can be seen in Figure 14, the heat of absorption of 17.7 m DGA is slightly higher than that of 3.6 m MOR + 14.7 m DGA. As a result more energy may be required to regenerate DGA than the blend solution.

## Solvent Losses

Vaporization losses are a direct result of alkanolamine vapor pressure in lean solvent. The predicted vapor pressure of MOR and DGA over 3.6 m MOR + 14.7 m DGA is presented in Figure 15. Since total pressures and gas phase compositions vary widely in industrial absorbers, results are presented as the vapor side fugacity of MOR. Since the gas leaving the absorber is in contact with the lean amine solution entering the top of the column, all calculations are done at a lean loading of 0.01 mol $CO_2$/mol amine. MOR is seen to be very volatile as compared to DGA.

## Conclusions

The carbamate of MOR is less stable than the carbamate of DGA by a factor of 7 to 10 from (300 to 333) K. The equilibrium $CO_2$ partial pressure over loaded 3.5 m MOR is greater that that of 17.7 m DGA and 3.6 m MOR + 14.7 m DGA. In addition, 3.6 m MOR + 14.7 m DGA has a higher equilibrium partial pressure of $CO_2$ at high loading by a factor of 5 to 7 than 17.7 m DGA. This is due to the low carbamate stability constant of MOR compared to DGA. Partial pressures

at low loading (< 0.1) in the blend are, however, similar to those in 17.7 m DGA. This is due to the stability of DGA and MOR carbamate.

The working capacity of 17.7 m DGA is ~17 % greater than the blend. Therefore 17.7 m DGA will require less solvent circulation than the blend. MOR vapor pressure is ~100 times greater than DGA vapor pressure at (313 to 333) K, potentially resulting in significant losses of MOR by evaporation. The regeneration energy of 3.6 m MOR + 14.7 m DGA will probably be less than 17.7 m DGA.

NMR has proven to be a useful technique in quantifying speciation. The most prevalent reaction product at high loading (> 0.5 at high loading) is MOR carbamate. The existence of the protonated DGA has the effect of stabilizing the overall MOR carbamate formation.

The model presented here is based on experimental results in 65 wt % amine (17.7 m DGA). Therefore care should be exercised when extrapolating these results to other amine concentrations.

## Literature Cited

(1) Harruff, L. G. The origin of morpholine in diglycolamine gas sweetening plants. *First International Conference on Chemistry in Industry*, Manama, Bahrain, 1992.
(2) Austgen, D. M. A model for vapor–liquid equilibrium for acid gas–alkanolamine–water systems. Ph.D. Dissertation, The University of Texas at Austin, Austin, TX, 1989.
(3) Posey, M. L. Thermodynamic model for acid gas loaded aqueous alkanolamine solutions. Ph.D. Dissertation, The University of Texas at Austin, Austin, TX, 1996.
(4) Pacheco M. A.; Kaganoi, S.; Rochelle, G. T. $CO_2$ absorption into aqueous mixtures of diglycolamine and methyldiethanolamine. *Chem. Eng. Sci.* **2000**, *55*, 5125–5140.
(5) Glasscock, D. A. Modelling and experimental study of carbon dioxide absorption into aqueous alkanolamines. Ph.D. Dissertation, The University of Texas at Austin, Austin, TX, 1990.
(6) Critchfield, J. E. $CO_2$ absorption/desorption in methyldiethanolamine solutions promoted with monoethanolamine and diethanolamine: mass transfer and reaction kinetics. Ph.D. Dissertation, The University of Texas at Austin, Austin, TX, 1988.
(7) Bishnoi, S.; Rochelle, G. T. Physical and chemical solubility of carbon dioxide in aqueous methyldiethanolamine. *Fluid Phase Equilib.* **2000**, *168*, 241–258.
(8) Austgen, D. M.; Rochelle, G. T.; Chen, C. C. Model of vapor–liquid equilibria for aqueous acid gas–alkanolamine systems using the electrolyte-NRTL equation. *Ind. Eng. Chem. Res.* **1989**, *28*, 1060.
(9) Posey, M. L.; Rochelle, G. T. A thermodynamic model of methyldiethanolamine–$CO_2$–$H_2S$–water. *Ind. Eng. Chem. Res.* **1997**, *36*, 3944–3958.
(10) Martin, J. L.; Otto, F. D., Mather, A. E. Solubility of hydrogen sulfide and carbon dioxide in a diglycolamine solution. *J. Chem. Eng. Data* **1978**, *23*, 163.
(11) Dingman, J. D.; Jackson, J. L.; Moore, T. F.; Branson, J. A. Equilibrium data for the $H_2S$–$CO_2$–diglycolamine agent–water system. *Proceedings of the Gas Processors Association Sixty-Second Annual Convention*, 1983.
(12) Versteeg, G. F.; Van Swaaij, W. P. M. Solubility and diffusivity of acid gases (carbon dioxide, nitrous oxide) in aqueous alkanolamine solutions. *J. Chem. Eng. Data* **1988**, *33*, 29–34.
(13) Bishnoi, S. Carbon dioxide absorption and solution equilibrium in piperazine activated methyldiethanolamine. Ph.D. Dissertation, The University of Texas at Austin, Austin, TX, 2000.
(14) Smith, W. R.; Missen, R. W. *Can. J. Chem. Eng.* **1988**, *66*, 591.
(15) Soave, G. Equilibrium constants from a modified Redlich–Kwong equation of state. *Chem. Eng. Sci.* **1972**, *27*, 1197.
(16) Chen, C. C.; Evans, L. B. A local composition model for the excess Gibbs energy of aqueous electrolyte systems. *AICHE J.* **1986**, *32*, 444–454.

(17) Chen, C. C.; Britt, H. I.; Boston, J. F.; Evans, L. B. Local composition model for excess Gibbs energy of electrolyte systems. Part I: Single solvent, single completely dissociated electrolyte systems. *AIChE J.* **1982**, *28*, 588−596.

(18) Chen, C. C.; Britt, H. I.; Boston, J. F.; Evans, L. B. Extension and application of the pitzer equation for vapor−liquid equilibrium of aqueous electrolyte systems with molecular solutes. *AIChE J.* **1979**, *25*, 820.

(19) Mock, B.; Evans, L. B.; Chen, C. C. Thermodynamic representation of phase equilibria of mixed-solvent electrolyte systems. *AIChE J.* **1986**, *32*, 1655−1664.

(20) Rowley, R. L.; Wilding, W. V.; Oscarson, J. L.; Adams, M. E.; Marshall, T. L. Physical and thermodynamic properties of pure chemicals: evaluated process design data: part 3; Design Institute for Physical Properties, AIChE: New York, 1999.

(21) Brelvi, S. W.; O'Connell, J. P. Correspondling states correlations for liquid compressibility and partial molal volumes of gases at infinite dilution in liquids. *AIChE J.* **1972**, *18*, 1239−1242.

(22) Stephenson, R. M., Malanowski, S., Eds. *Handbook of the Thermodynamics of Organic Compounds*; Elsevier Science Publishing Co.: New York, 1987.

(23) Vistad, O. B.; Akporiaye, D. E.; Taulelle, F.; Lillerud, K. P. In situ NMR of SAPO-34 crystallization. *Chem. Mater.* **2003**, *15*, 1650−1654.

(24) Harruff, L. G.; Saudi Arabian experience with DGA units and related sulfur plants. In *Proceedings of the Laurence Reid Gas Conditioning Conference*, 1998.

(25) Smith, J. M., Van Ness, H. C., Eds. *Introduction to Chemical Engineering Thermodynamics*; McGraw-Hill Book Co.: New York, 1975.

(26) Al-Juaied, M. Carbon dioxide removal from natural gas by membranes in the presence of heavy hydrocarbons and by aqueous diglycolamine/morpholine. Ph.D. Dissertation, The University of Texas at Austin, Austin, TX, 2004.

(27) Perrin, D. D. *pKa Prediction for Organic Acids and Bases*; Chapman and Hall: London−New York, 1981.

(28) Caplow, M. Kinetics of carbamate formation and breakdown. *J. Am. Chem. Soc.* **1968**, *90*, 6795.

(29) Wu, H. S.; Locke, W. E.; Sandler, S. I. Isothermal vapor−liquid equilibrium of binary mixtures containing morpholine. *J. Chem. Eng. Data* **1991**, *36*, 127−130.

(30) Wilson, H. L.; Wilding, W. V. In *Experimental Results for DIPPR 1990−91 Projects on Phase Equilibria and Pure Components Properties*, No. 2; Cunningham, J. R., Jones, D. K., Eds.; American Institute of Chemical Engineers: New York, 1994.

(31) Dohnal, V.; Roux, A. H.; Hynek, V. Limiting partial molar excess enthalpies by flow calorimetry: some organic solvents in water, *J. Solution Chem.* **1994**, *23*, 889−900.